

Tunable THz Surface Plasmon Polariton based on Topological Insulator-Layered Superconductor Hybrid Structure

Mingda Li,^{1,*} Zuyang Dai,² Wenping Cui,³ Zhe Wang,¹
Ferhat Katmis,⁴ Peisi Le,¹ Jiayue Wang,⁵ Lijun Wu,⁶ and Yimei Zhu⁶

¹*Department of Nuclear Science and Engineering, Massachusetts Institute of Technology,
77 Massachusetts Avenue, Cambridge, MA 02139, USA*

²*Department of Physics, Tsinghua University, Beijing 10084, China*

³*Institut für Theoretische Physik, Universität zu Köln, Zùlpicher Str. 77, D-50937 Köln, Germany*

⁴*Department of Physics, Massachusetts Institute of Technology,
77 Massachusetts Avenue, Cambridge, MA 02139, USA*

⁵*Department of Engineering Physics, Tsinghua University, Beijing 10084, China*

⁶*Department of Condensed Matter Physics, Brookhaven National Lab, Upton, New York 11973, USA*

(Dated: November 5, 2018)

We theoretically investigate the surface plasmon polariton (SPP) at the interface between 3D strong topological insulator (TI) and layered superconductor-magnetic insulator structure. The tunability of SPP through electronic doping can be enhanced when the magnetic permeability of the layered structure becomes higher. When the interface is gapped by superconductivity or perpendicular magnetism, SPP dispersion is further distorted, accompanied by a shift of group velocity and penetration depth. Such a shift of SPP reaches maximum when the magnitude of Fermi level approaches the gap value, and may lead to observable effects. The tunable SPP at the interface between layered superconductor and magnetism materials in proximity to TI surface may provide new insight in the detection of Majorana Fermions.

I. INTRODUCTION

Surface plasmon polariton (SPP) is the collective excitation of electrons at the interface between conductor and dielectrics driven by electromagnetic (EM) waves.^{1,2} Despite its wide applications in nanophotonics³, near-field optics and tip-enhanced Raman spectroscopy^{4,5}, and biological sensors and antennas^{6,7}, SPP in general suffers from problem of huge non-radiative loss due to the strong absorption of the metal¹⁻⁴ accompanied with additional radiative loss⁸, which limits SPP's lifetime and propagation length for further application in integrated devices.

In order to solve the SPP loss problem, the low-loss plasmonics based on graphene⁹⁻²³ and topological insulators (TI)²⁴⁻³¹ has attracted much recent attention. In far infrared and THz range, the major loss mechanism in graphene lies in the scattering between electrons and optical phonons¹¹. A number of studies in graphene plasmonics have been conducted utilizing the properties of low loss and tunability. Yan *et al.*³² have reported enhanced plasmon resonance in patterned graphene-insulator stack structure comparing with single-layered graphene, while Ju *et al.*¹² demonstrated an enhanced tunability at THz range in micro-ribbon graphene metamaterials. These efforts target at manipulation of photons and miniaturization of optical devices, and could be further integrated and hybridized toward further applications in detectors, modulators or other integrated devices.

On the other hand, in doped 3D TI, the electron-impurity scattering becomes dominant due to weak electron-phonon coupling²⁸, with a further reduced backscattering probability thanks to topological protected surface states³³⁻³⁵. However, unlike the boom-

ing studies in graphene plasmonics, the plasmon hybrid devices in TI have been seldom reported, even with comparable performance in THz range as well as additional features such as net spin polarization, i.e. "spin plasmon"^{24-26,31} and spin-charge separation³⁰.

Therefore, in this paper, we propose a plasmonic hybrid structure composed of 3D TI in close contact with layered superconductor. This structure provides a new platform where SPP waves are supported. The tunability of the SPP propagation can be achieved independently through either gate voltage and magnetic field. Since the Majorana bound states, which are an non-Abelian anyons in superconductors and may have great impact in topological quantum computation³⁴, may exist at the boundary of 3D TI and superconductor, this plasmonic structure may provide a new perspective in search for Majorana bound states.

II. THEORY

A. Dispersion Relation of Anisotropic SPP Wave

Since the SPP wave is localized along the interface, and the Dirac electrons only exist on the surface of TI, we use anisotropic dielectric functions to model the dielectric function of a 3D TI in order to capture both the Dirac dielectric functions of 2D chiral Dirac electrons at the surface (Fig. 1, xy plane, $z = 0$) as well as the dielectric constant in the bulk (Fig. 1, $z > 0$ region).

In order to describe wave propagation in the layered structure (Fig. 1 $z < 0$ region), we adopt the method proposed by Averkov *et al.*³⁶ using anisotropic dielectric function. This is valid when $\lambda_{SP} \gg D$, where λ_{SP} is the

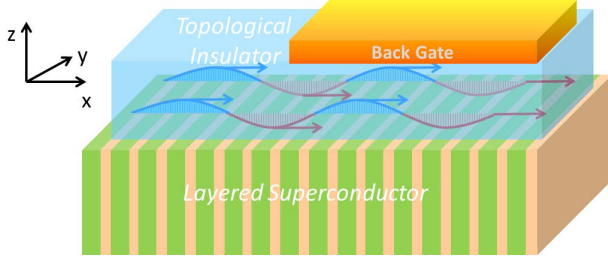


FIG. 1. The schematic configuration of 3D TI-layered superconductor hybrid structure. The $z < 0$ region consist of alternating layers of superconductor and nonmagnetic or magnetic insulator. The SPP wave propagates along the interface. A back gate is present to tune the Fermi level of the interfacial electrons, which leads to a change of dielectric functions and furthermore a change of SPP propagation properties.

SPP wavelength, and D is the spatial periodicity of the layered structure. Since we are interested in long wavelength THz range, the condition that $\lambda_{SP} \gg D$ is guaranteed to meet. In this approach, the anisotropy leads to the existence of optical axis where EM wave suffers no birefringence³⁷. Thus the electric field and magnetic field at the interface can be written as a superposition of ordinary wave and extraordinary wave:

$$\begin{cases} \mathbf{E}_j = \left(\mathbf{E}_j^o e^{-\kappa_j^o |z|} + \mathbf{E}_j^e e^{-\kappa_j^e |z|} \right) e^{i(q_x x + q_y y - \omega t)} \\ \mathbf{H}_j = \left(\mathbf{H}_j^o e^{-\kappa_j^o |z|} + \mathbf{H}_j^e e^{-\kappa_j^e |z|} \right) e^{i(q_x x + q_y y - \omega t)} \end{cases} \quad (1)$$

where $j = 1, 2$ is for the TI and layered superconductor side, respectively. Based on our model, the TI dielectric function is defined as $\varepsilon_1 = (\varepsilon_{2D}(q, \omega), \varepsilon_{2D}(q, \omega), \varepsilon_d)$ with optical axis along z direction, while the dielectric function of layered superconductor is defined as $\varepsilon_2 = (\varepsilon_c(q, \omega), \varepsilon_{ab}(q, \omega), \varepsilon_{ab}(q, \omega))$, which is anisotropic along x direction.

By noticing the different direction of optical axis in the upper TI region and lower superconductor region, that for ordinary wave and extraordinary wave we have $E_{1z}^o = 0$, $E_{2x}^e = 0$, and $H_{1z}^o = 0$, $H_{2x}^e = 0$, respectively. The x components of the EM fields are shown in Appendix A, with light speed in vacuum $c = 1$ and μ is the magnetic permeability of the layered superconductor material.

Substituting the EM field components back to eq. (1), we obtain the localization constants, i.e. inverse of penetration depth away from the interface.

$$\kappa_1^o = \sqrt{q_x^2 + q_y^2 - \varepsilon_{2D}(q, \omega)\omega^2} \quad (2)$$

$$\kappa_1^e = \sqrt{\varepsilon_{2D}(q, \omega) \left(\frac{q_x^2 + q_y^2}{\varepsilon_d} - \omega^2 \right)} \quad (3)$$

$$\kappa_2^o = \sqrt{q_x^2 + q_y^2 - \mu \varepsilon_{ab}(q, \omega)\omega^2} \quad (4)$$

$$\kappa_2^e = \sqrt{\frac{\varepsilon_c(q, \omega)}{\varepsilon_{ab}(q, \omega)} q_x^2 + q_y^2 - \mu \varepsilon_c(q, \omega)\omega^2} \quad (5)$$

The dispersion relation of the resulting surface wave can

be written in a determinant form:

$$\begin{vmatrix} -i\kappa_1^o & \frac{i\omega^2 \varepsilon_1}{\kappa_1^o} & -\frac{q_y^2 - (\kappa_2^o)^2}{i\mu\kappa_2^o} & 0 \\ -q_y^2 & q_x^2 & 0 & -q_x^2 + \mu\omega^2 \varepsilon_{ab} \\ \kappa_1^o q_y^2 & \frac{\omega^2 q_x^2 \varepsilon_1}{\kappa_1^o} & \frac{q_x^2 q_y^2}{\mu\kappa_2^o} & \omega^2 \varepsilon_{ab} \kappa_2^e \\ 1 & 1 & -1 & -1 \end{vmatrix} = 0 \quad (6)$$

In this paper, we only consider the wave propagating along x direction, neglecting the oblique excitation. The dispersion relation can finally be simplified as

$$q = \omega \sqrt{\frac{\varepsilon_d \varepsilon_{ab}(q, \omega) [\varepsilon_c(q, \omega) - \mu \varepsilon_{2D}(q, \omega)]}{\varepsilon_c(q, \omega) \varepsilon_{ab}(q, \omega) - \varepsilon_{2D}(q, \omega) \varepsilon_d}} \quad (7)$$

which is the main analytical result. In this expression, μ is the effective permeability of the layered superconductor structure, q is the wavenumber along x direction, and can be a complex number. When both the upper and lower materials are isotropic, i.e. $\varepsilon_{2D} = \varepsilon_d = \varepsilon_1$ and $\varepsilon_{ab} = \varepsilon_c = \varepsilon_2$, it is further reduced to the well-known result $q = \omega \sqrt{\frac{\varepsilon_1 \varepsilon_2}{\varepsilon_1 + \varepsilon_2}}$.

B. Dielectric Function of Layered Superconductor

Define dimensionless frequency $\Omega = \omega/\omega_J$, with ω_J the Josephson plasmon frequency of the layered superconductor, the dielectric function of layered superconductor can be written as³⁶:

$$\varepsilon_c(\Omega) = \varepsilon_s \left(1 - \frac{1}{\Omega^2} \right), \quad \varepsilon_{ab}(\Omega) = \varepsilon_s \left(1 - \frac{\gamma^2}{\Omega^2} \right) \quad (8)$$

where the imaginary parts are neglected. Throughout this article, we take the value reported in³⁶ and set the interlayer dielectric constant $\varepsilon_s = 16$, current-anisotropy parameter $\gamma = 200$ and $\omega_J = 4$ meV.

C. Dielectric Function of Gapless Topological Insulator

The dielectric function of the chiral gapless topological insulator surface have been reported in^{24,25,27}, where for the Hamiltonian for 2D helical Dirac electron gas H_0 :

$$H_0 = \hbar v_F \sum_k \Psi_k^\dagger \left(\hat{z} \times \vec{k} \right) \cdot \vec{\sigma} \Psi_k \quad (9)$$

the Lindhard Dielectric function $\varepsilon_{2D}(q, \omega)$ can be written as

$$\varepsilon_{2D}(q, \omega) = 1 - V_{2D}(q) \Pi(q, \omega) = 1 - \frac{e^2}{2\varepsilon_0 q} \Pi(q, \omega) \quad (10)$$

with the polarization operator

$$\Pi(q, \omega) = \frac{g}{4\pi^2} \sum_{\gamma, \gamma'} \int d\mathbf{k} \frac{n_{\mathbf{k}, \gamma} - n_{\mathbf{k}+\mathbf{q}, \gamma'}}{\hbar\omega + E_{\mathbf{k}, \gamma} - E_{\mathbf{k}+\mathbf{q}, \gamma'} + i\delta} |\langle f_{\mathbf{k}, \gamma} | f_{\mathbf{k}+\mathbf{q}, \gamma'} \rangle|^2 \quad (11)$$

In this expression, g is the spin/valley degeneracy, for the chiral states we have $g = 1$ due to spin-momentum locking, $n_{\mathbf{k}, \gamma}$ is Fermi occupation value at energy eigenvalue, $E_{\mathbf{k}, \gamma} = \gamma \hbar v_F k$, with $\gamma = 1$ for conduction band and $\gamma = -1$ for valence band, respectively. The spinor eigenstates $|f_{\mathbf{k}, \gamma}\rangle = (e^{-i\theta_{\mathbf{k}}/2}, i\gamma e^{i\theta_{\mathbf{k}}/2})/\sqrt{2}$, with $\theta_{\mathbf{k}}$ defined as $\tan \theta_{\mathbf{k}} = k_y/k_x$. We take the value of Fermi velocity $v_F = 6.2 \times 10^5$ m/s³⁸ in all calculations.

Eq. (11) can be calculated either analytically^{27,39} or numerically, thanks to the identical expression of polarization operator within RPA for simple Dirac gas and helical Dirac gas. In our approach, we choose $T = 10$ K for numerical integration to avoid discontinuity, and compare with analytical result with at least 6 digit agreement. Then the numerical result for gapless TI is applied

$$H_{BdG} = \frac{1}{2} \sum_{\mathbf{k}} \Psi_{\mathbf{k}}^+ \begin{pmatrix} k_x \sigma_y - k_y \sigma_x + M \sigma_z - E_F & i|\Delta| \sigma_y \\ -i|\Delta| \sigma_y & -k_x \sigma_y - k_y \sigma_x - M \sigma_z - E_F \end{pmatrix} \Psi_{\mathbf{k}} \quad (12)$$

where spinor $\Psi_{\mathbf{k}} = (c_{\mathbf{k}\uparrow}, c_{\mathbf{k}\downarrow}, c_{-\mathbf{k}\uparrow}^+, c_{-\mathbf{k}\downarrow}^+)$ and denote the magnetic gap and superconductivity gap, respectively, E_F is the chemical potential. Both eq. (10) and eq. (11) still hold, but the eigenvalues and eigenvectors are changed. The eigenvalues can now be written as

$$\begin{aligned} E_1 &= \sqrt{|\Delta|^2 + 2(|\Delta|^2 M^2 + E_F^2 M^2 + E_F^2 k^2)^{1/2} + M^2 + k^2 + E_F^2} \\ E_2 &= \sqrt{|\Delta|^2 - 2(|\Delta|^2 M^2 + E_F^2 M^2 + E_F^2 k^2)^{1/2} + M^2 + k^2 + E_F^2} \\ E_3 &= -\sqrt{|\Delta|^2 - 2(|\Delta|^2 M^2 + E_F^2 M^2 + E_F^2 k^2)^{1/2} + M^2 + k^2 + E_F^2} \\ E_4 &= -\sqrt{|\Delta|^2 + 2(|\Delta|^2 M^2 + E_F^2 M^2 + E_F^2 k^2)^{1/2} + M^2 + k^2 + E_F^2} \end{aligned}$$

The corresponding unnormalized eigenvectors are shown in Appendix A.

When the surface state is gapped, the EM constitutive relations have been modified with an additional axion term⁴¹ and leads to electromagnetic effect. However, it is shown that such effect^{41,42} only has $\sim \alpha^2$ correction to the SPP dispersion, where α is the fine structure constant, thus in the present calculation we neglect the effect from axion electrodynamics

III. RESULTS AND DISCUSSIONS

In order to conveniently express the dielectric functions for both TI and layered superconductor, we define

to solve for the dielectric function of TI when surface state is gapped.

D. Dielectric Function of Gapped Topological Insulator

Either the magnetic field perpendicular to the interface (along z direction in Fig. 1) or the superconductivity would open up a gap to the gapless Dirac cone, and lift out the degeneracy at $k = 0$, and further alter the dielectric function as well SPP dispersions. In order to take the effect of gaps into account, we adopt the Bogoliubov-de Gennes Hamiltonian^{33,40}, which can be regarded as a generalization of eq. (8):

dimensionless wavenumber $Q = v_F q_x / (c\omega_J)$, and all energies are dimensionless and expressed in the unit of ω_J .

The SPP dispersion relations are obtained by solving Eq. (7). The typical dispersion relations at various gate voltages, i.e. Fermi levels E_F , are shown in Fig. 2 a and b. We see an enhanced tunability, i.e. shift of dispersion relation when E_F varies, when the lower layer has increased effective magnetic permeability μ . By defining the SPP group velocity $v_g = d\Omega/dQ$, we see an additional change of propagation properties induced by either M or $|\Delta|$ (Fig. 2 c and d) by plotting the percentage SPP group velocity shift

$$\frac{\Delta v_g}{v_g} = \frac{v_g(\text{gapped}) - v_g(\text{gapless})}{v_g(\text{gapless})}$$

Here both the magnetic gap M and superconductivity gap $|\Delta|$ are dimensionless in the unit of Josephson plasmon frequency ω_J .

In order to further investigate the effect of gap to the SPP propagation, the relative shift of group velocity $\Delta v_g/v_g$ as a function of dimensionless wavenumber Q and Fermi level E_F are shown in Fig. 3, at different values of gap. It can be seen directly that the shift is increased at larger gap value, and it increases as a function of Q . Most importantly, the shift reaches peak value when the Fermi level approaches to the gap value. This feature can be seen more clearly in a line plot with fixed Q value (Fig. 3 d). We also see that SPP group velocity v_g does not shift when Fermi level $E_F = 0$. In contrary

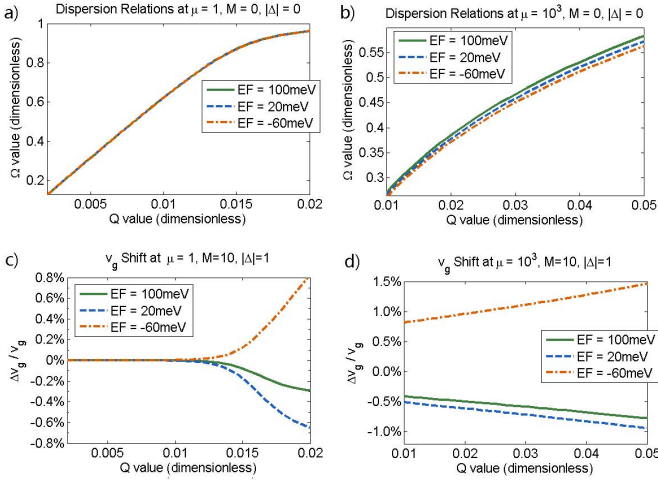


FIG. 2. The dispersion relations (a-b) and gap-induced group velocity changes (c-d) of SPP at various Fermi levels with respect to gap opening. The Fermi levels are taken at 3 different values with 80 meV interval. In c), at $\mu = 1$, even if the tuning of Fermi level does not change much to the dispersion relation itself as shown in a), it still shows a shift to SPP group velocity at high Q range.

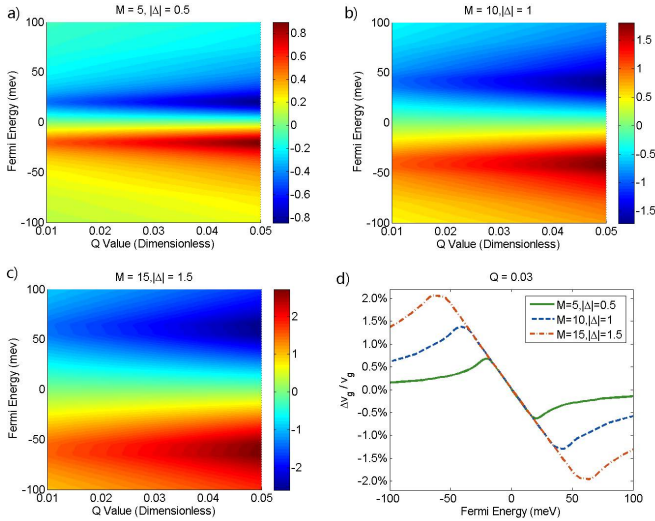


FIG. 3. The percentage shift of SPP group velocity as a function of Q and E_F , at 3 different gap values $M = 5$ $|\Delta| = 0.5$ (a), $M = 10$ $|\Delta| = 1.0$, (b) and $M = 15$ $|\Delta| = 1.5$, (c). The change is negative for $E_F > 0$ and positive for $E_F < 0$, and reaches maximum when the Fermi level is close to the gap values (d). Notice all gap values are expressed in the unit of ω_J ($\omega_J = 4$ meV throughout calculation), for instance the green solid line $M = 5$ $|\Delta| = 0.5$ corresponds to $M = 20$ meV $|\Delta| = 2$ meV.

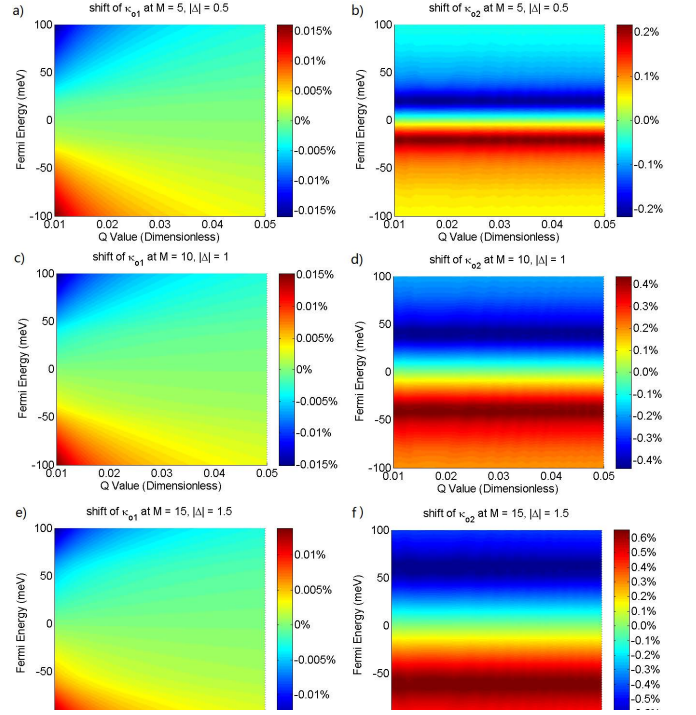


FIG. 4. Relative shift of o-light component of localization constants for TI $\kappa_1^{(o)}$ (figs a, c, e), and layered superconductor $\kappa_2^{(o)}$ (figs b, d, f). The localization constants for e-light $\kappa_1^{(e)}$ and $\kappa_2^{(e)}$ have different magnitudes but similar feature of $\kappa_1^{(o)}$ and $\kappa_2^{(o)}$, respectively. We see that the shift is not sensitive to Fermi level E_F of topological insulators, but always reaches peak values when E_F is near the value of gap. Unlike the shift of group velocity, which is Q dependent, the localization constants are almost independent Q value.

to the Q and E_F dependent shift of group velocity caused by energy gap, the localization constants show a qualitatively different behavior. The localization constant in TI side $\kappa_1^{(o)}$ is neither sensitive to E_F nor to Q (Fig. 4 a, c, e), while in layered superconductor side, $\kappa_2^{(o)}$ is tunable by E_F but still Q -independent. The importance of the localization constant shift as Q can hardly be overestimated, in that it indicates that the different propagation properties of SPP is almost fully coming from the group velocity, other than the difference in SPP wavelength. The fewer controllable variables would indefinitely make the experimental results easier to explain.

The reason that the maximum v_g shift occurs when the gap matches the Fermi level can be understood in the light of electronic transition and available electron density for plasmonic oscillation. Electrons in the conduction band are mostly extended and dominate the surface plasmon excitation. When the Fermi level is lower than the energy gap, charge carriers need additional energy to fulfill the transition to the conduction band in order to contribute to the collective excitation. On the other hand, since the SPP is excited by EM waves, when the

Fermi level is higher than the energy gap, the electronic transition by optical excitation is limited by occupied electrons. The increasing forbidden transition leads to a reduced shift of dielectric function, and moreover the v_g shift is reduced accordingly. Thus, only when the Fermi level reaches the value of energy gap are the number of available electrons participating in the electronic transition and collective excitation maximized, and leads to a shift of SPP frequency and group velocity.

IV. CONCLUSIONS

We provide a generic theoretical framework to study the surface plasmon polariton (SPP) at the interface between topological insulator (TI) and layered superconductors. The SPP in this hybrid structure may be widely applied to study novel optical and transport phenomena at the interface, through the tunability of SPP propagation by gating or gapping the surface states of the TI. It can also be generalized to a larger category of materials in proximity to TI surface. For instance, Wei *et al.*^{43,44} have shown that when the ferromagnetic insulator EuS is on the top of topological insulator Bi₂Se₃, it induces significant magnetic moment in Bi₂Se₃ thin films and induces breaking of T-reversal symmetry. The SPP in such Ferromagnetic- TI hybrid structure can also be studied within this approach.

Furthermore, Majorana zero mode is predicted to exist^{35,40,45} as a domain wall state at the interface between TI and ferromagnetic-superconductor boundaries. Therefore, at the TI-layered superconductor interface, propagating SPP may interact with the Majorana domain wall state, and leads to the shift of the SPP propagation properties, including group velocity, reflectivity and transmissivity, etc. In this regards, the change of optical properties of SPP can be considered a semi-classical manifestation of the existence of Majorana fermions, which is a pure quantum phenomenon with non-Abelian statistics. The existence of the zero mode level may contribute to electronic transition, and leads to a further change of dielectric functions. Unlike transport measurements, which involve only a single Majorana fermion domain wall state, this hybrid structure can be regarded as the interaction between SPP and a series of domain wall states, coming from each domain wall state along the interface. In a nutshell, the SPP on the TI surface may provide insights to the detection of Majorana Fermions as a conceptually novel platform.

ACKNOWLEDGMENTS

Author Mingda Li would thank Prof. Ju Li for his generous support and helpful discussions.

Appendix A: Components of EM Fields

$$H_{1x}^{(o)} = \frac{\kappa_1^{(o)}}{i\omega} E_{1y}^{(o)}, E_{1x}^{(o)} = -\frac{q_y}{q_x} E_{1y}^{(o)}, H_{1y}^{(o)} = -\frac{i\kappa_1^{(o)} q_y}{\omega q_x} E_{1y}^{(o)}$$

$$H_{1z}^{(o)} = \frac{q_x^2 + q_y^2}{\omega q_x} E_{1y}^{(o)}, H_{1x}^{(e)} = \frac{i\omega \varepsilon_{2D}(q, \omega)}{\kappa_1^{(e)}} E_{1y}^{(e)}, E_{1x}^{(e)} = \frac{q_x}{q_y} E_{1y}^{(e)}$$

$$H_{1y}^{(e)} = -\frac{i\omega q_x \varepsilon_{2D}(q, \omega)}{q_y \kappa_1^{(e)}} E_{1y}^{(e)}, E_{1z}^{(e)} = \left(\frac{i\kappa_1^{(e)}}{q_y} + \frac{i\omega^2 \varepsilon_{2D}(q, \omega)}{q_y \kappa_1^{(e)}} \right) E_{1y}^{(e)}$$

$$H_{2z}^{(o)} = \frac{q_x}{\omega \mu} E_{2y}^{(o)}, H_{2y}^{(o)} = \frac{i q_x q_y}{\omega \mu \kappa_2^{(o)}} E_{2y}^{(o)}, E_{2z}^{(o)} = -\frac{i q_y}{\kappa_2^{(o)}} E_{2y}^{(o)}$$

$$H_{2x}^{(o)} = \frac{q_y^2 - (\kappa_2^{(o)})^2}{i\omega \mu \kappa_2^{(o)}} E_{2y}^{(o)}, E_{2z}^{(e)} = \frac{\kappa_2^{(e)}}{i q_y} E_{2y}^{(e)}, H_{2z}^{(e)} = \frac{\omega \varepsilon_{ab}(q, \omega)}{q_x} E_{2y}^{(e)}$$

$$H_{2y}^{(e)} = -\frac{\omega \varepsilon_{ab}(q, \omega) \kappa_2^{(e)}}{i q_x q_y} E_{2y}^{(e)}, E_{2x}^{(e)} = \frac{q_x^2 - \mu \omega^2 \varepsilon_{ab}(q, \omega)}{q_x q_y} E_{2y}^{(e)}$$

Appendix B: (Un-normalized) Eigenvectors of BdG Hamiltonian

Define $k^2 = k_x^2 + k_y^2$, $\delta^- = |\Delta| - M$ and $\delta^+ = |\Delta| + M$, the four eigenvectors can be written as:

$$\begin{aligned} |f_{\mathbf{k},1}\rangle &= \left(-1, \frac{\delta^- + \sqrt{(\delta^-)^2 + k^2}}{i k_x + k_y}, -\frac{\delta^- + \sqrt{(\delta^-)^2 + k^2}}{i k_x + k_y}, 1 \right)^T \\ |f_{\mathbf{k},2}\rangle &= \left(1, \frac{\delta^+ - \sqrt{(\delta^+)^2 + k^2}}{i k_x + k_y}, \frac{\delta^+ - \sqrt{(\delta^+)^2 + k^2}}{i k_x + k_y}, 1 \right)^T \\ |f_{\mathbf{k},3}\rangle &= \left(-1, \frac{\delta^- - \sqrt{(\delta^-)^2 + k^2}}{i k_x + k_y}, \frac{-\delta^- + \sqrt{(\delta^-)^2 + k^2}}{i k_x + k_y}, 1 \right)^T \\ |f_{\mathbf{k},4}\rangle &= \left(1, \frac{\delta^+ + \sqrt{(\delta^+)^2 + k^2}}{i k_x + k_y}, \frac{\delta^+ + \sqrt{(\delta^+)^2 + k^2}}{i k_x + k_y}, 1 \right)^T \end{aligned}$$

* Author to whom correspondence should be addressed:

- ¹ J. Pitarke, V. Silkin, E. Chulkov, and P. Echenique, Reports on progress in physics **70**, 1 (2007).
- ² S. A. Maier, *Plasmonics: Fundamentals and Applications: Fundamentals and Applications* (Springer, 2007).
- ³ S. P. Nanophotonics, *Springer Series in Optical Sciences Vol. 131, edited by PG Kik and ML Brongersma* (Springer, Dordrecht, 2007).
- ⁴ S. Kawata, *Near-field optics and surface plasmon polaritons*, Vol. 20 (Springer, 2001).
- ⁵ W. Cui, M. Li, Z. Dai, Q. Meng, and Y. Zhu, The Journal of Chemical Physics **140**, 044109 (2014).
- ⁶ J. Homola, *Surface plasmon resonance based sensors*, Vol. 4 (Springer, 2006).
- ⁷ J. Becker, *Plasmons as sensors* (Springer, 2012).
- ⁸ T. Vary and P. Markoř, Opto-Electronics Review **18**, 400 (2010).
- ⁹ B. Wunsch, T. Stauber, F. Sols, and F. Guinea, New Journal of Physics **8**, 318 (2006).
- ¹⁰ E. Hwang and S. D. Sarma, Physical Review B **75**, 205418 (2007).
- ¹¹ M. Jablan, H. Buljan, and M. Soljačić, Physical review B **80**, 245435 (2009).
- ¹² L. Ju, B. Geng, J. Horng, C. Girit, M. Martin, Z. Hao, H. A. Bechtel, X. Liang, A. Zettl, Y. R. Shen, *et al.*, Nature nanotechnology **6**, 630 (2011).
- ¹³ F. H. Koppens, D. E. Chang, and F. J. Garcia de Abajo, Nano letters **11**, 3370 (2011).
- ¹⁴ H. Yan, F. Xia, Z. Li, and P. Avouris, New Journal of Physics **14**, 125001 (2012).
- ¹⁵ A. Grigorenko, M. Polini, and K. Novoselov, Nature photonics **6**, 749 (2012).
- ¹⁶ S. A. Maier, Nature Physics **8**, 581 (2012).
- ¹⁷ Q. Bao and K. P. Loh, ACS nano **6**, 3677 (2012).
- ¹⁸ P. Tassin, T. Koschny, M. Kafesaki, and C. M. Soukoulis, Nature Photonics **6**, 259 (2012).
- ¹⁹ V. W. Brar, M. S. Jang, M. Sherrott, J. J. Lopez, and H. A. Atwater, Nano letters **13**, 2541 (2013).
- ²⁰ D. Jin, A. Kumar, K. H. Fung, J. Xu, and N. X. Fang, Applied Physics Letters **102**, 201118 (2013).
- ²¹ W. B. Lu, W. Zhu, H. J. Xu, Z. H. Ni, Z. G. Dong, and T. J. Cui, Optics express **21**, 10475 (2013).
- ²² H. Buljan, M. Jablan, and M. Soljačić, Nature Photonics **7**, 346 (2013).
- ²³ P. Avouris and M. Freitag, Selected Topics in Quantum Electronics, IEEE Journal of **20**, 72 (2014).
- ²⁴ D. K. Efimkin, Y. E. Lozovik, and A. A. Sokolik, Nanoscale research letters **7**, 1 (2012).
- ²⁵ D. Efimkin, Y. E. Lozovik, and A. Sokolik, Journal of Magnetism and Magnetic Materials **324**, 3610 (2012).
- ²⁶ O. Roslyak, G. Gumbs, and D. Huang, Physical Review B **87**, 045121 (2013).
- ²⁷ R. Schütky, C. Ertler, A. Trügler, and U. Hohenester, Physical Review B **88**, 195311 (2013).
- ²⁸ P. Di Pietro, M. Ortolani, O. Limaj, A. Di Gaspare, V. Giliberti, F. Giorgianni, M. Brahlek, N. Bansal, N. Koirala, S. Oh, *et al.*, Nature nanotechnology **8**, 556 (2013).
- ²⁹ Y. Okada and V. Madhavan, Nature nanotechnology **8**, 541 (2013).
- ³⁰ T. Stauber, G. Gómez-Santos, and L. Brey, Physical Review B **88**, 205427 (2013).
- ³¹ C. Chen, Z. Xie, Y. Feng, H. Yi, A. Liang, S. He, D. Mou, J. He, Y. Peng, X. Liu, *et al.*, Scientific reports **3** (2013).
- ³² H. Yan, X. Li, B. Chandra, G. Tulevski, Y. Wu, M. Freitag, W. Zhu, P. Avouris, and F. Xia, Nature nanotechnology **7**, 330 (2012).
- ³³ B. A. Bernevig, *Topological Insulators and Topological Superconductors* (Princeton University Press, 2013).
- ³⁴ M. Z. Hasan and C. L. Kane, Reviews of Modern Physics **82**, 3045 (2010).
- ³⁵ X.-L. Qi and S.-C. Zhang, Reviews of Modern Physics **83**, 1057 (2011).
- ³⁶ Y. O. Averkov, V. M. Yakovenko, V. A. Yampol'skii, and F. Nori, Phys. Rev. B **87**, 054505 (2013).
- ³⁷ E. Hecht, Optics, 4th Edition, Addison Wesley Longman Inc, 1998 **1** (1998).
- ³⁸ H. Zhang, C.-X. Liu, X.-L. Qi, X. Dai, Z. Fang, and S.-C. Zhang, Nature physics **5**, 438 (2009).
- ³⁹ E. Hwang and S. D. Sarma, Physical Review B **75**, 205418 (2007).
- ⁴⁰ L. Fu and C. L. Kane, Physical Review Letters **100**, 096407 (2008).
- ⁴¹ A. Karch, Physical Review B **83**, 245432 (2011).
- ⁴² M. Li, W. Cui, L. Wu, Q. Meng, Y. Zhu, Y. Zhang, W. Liu, and Z. Ren, arXiv preprint arXiv:1309.6198 (2013).
- ⁴³ P. Wei, F. Katmis, B. A. Assaf, H. Steinberg, P. Jarillo-Herrero, D. Heiman, and J. S. Moodera, Phys. Rev. Lett. **110**, 186807 (2013).
- ⁴⁴ P. Wei, F. Katmis, D. Assaf, Badih and Heiman, and J. Moodera, in *APS Meeting Abstracts*, Vol. 1 (2013) p. 13007.
- ⁴⁵ L. Fu and C. L. Kane, Physical review letters **102**, 216403 (2009).